Applied Physics B (2024) 130:171
https://doi.org/10.1007/s00340-024-08311-z

RESEARCH

Passively Q-switched Tm:YAP laser based on WSe_2/CuO heterojunction saturable absorber

Yiheng Yang[1] · Lulu Gao[2] · Yingxue Han[1] · Qiong Gao[1] · Ruijun Lan[2] · Yingjie Shen[2]

Received: 1 August 2024 / Accepted: 26 August 2024

Abstract

WSe_2 and CuO belong to transition metal chalcogenides (TMDs) and transition metal oxides (TMOs), respectively, and both are semiconductor materials that have been applied in production in many fields. In this work, WSe_2/CuO heterojunction nanocomposites were prepared by simple and non-toxic liquid phase exfoliation (LPE) and vacuum filtration methods, and WSe_2/CuO heterojunction saturable absorber (SA) devices were prepared by film transfer technology. The morphology and purity of the WSe_2/CuO heterojunction were studied. In addition, the WSe_2/CuO heterojunction SA was applied to a passively Q-switched (PQS) solid-state laser for the first time, generating a stable pulse output with a Watt-level output power, a maximum average output power of 2.32 W, a repetition frequency of 68.68 kHz, and a minimum pulse width of 752.8 ns. Our research results illustrate the great potential and broad application prospects of WSe_2/CuO composites in the field of photonic devices.

1 Introduction

Two-dimensional materials with many excellent properties (such as mechanical properties, electrical properties, and optical properties) have rapidly emerged in recent years, prompting researchers to study them [1–3]. Two-dimensional materials have also promoted the production and development of many fields such as nonlinear optics, photoelectron catalysis, batteries, and chips [4–7]. In particular, the saturable absorption characteristics of two-dimensional materials enable them to play an important role as core modulation devices in the field of ultrashort pulse lasers [8–13]. Transition metal chalcogenides (TMDs) are a class of layered two-dimensional materials with excellent performance. The inherent adjustable band gap that changes with the number of layers has become an important and irreplaceable feature that plays an important role in many fields [14–17]. This feature also proves their application potential in the field of optoelectronic devices. At present, researchers have successfully manufactured a large number of high-performance optoelectronic devices using TMDs [18–22]. As a member of the widely studied V-group TMDs family, WSe_2 has an extremely high nonlinear two-photon absorption coefficient (1.9×10^{-9} cm/W) and a wide bandgap change from an indirect bandgap of 1.2 eV in bulk materials to a direct bandgap of 1.65 eV in monolayer materials, which enables it to fully demonstrate the powerful ability of passively modulated ultrashort pulse lasers in a wide near-infrared band [23]. In recent years, transition metal oxides (TMOs) similar to TMDs have also set off a wave of research due to their non-toxic, high stability, conductivity, and wide-band optical properties [24–29]. In the field of optoelectronic devices, CuO is the most representative member, and has received extensive attention and research due to its excellent properties such as high stability, nonlinear optical properties, ultrashort recovery time, and narrow bandgap [30]. However, there are few studies on CuO as a saturable absorber (SA) in the field of pulsed lasers. At present, the use of a single material cannot meet the needs of research in various fields. In order to improve performance, researchers have found that the performance of van der Waals heterojunction is more prominent, and the

✉ Qiong Gao
gaoqiong1988@hrbun.edu.cn

✉ Yingjie Shen
yingjieyj@163.com

[1] Key Laboratory of Photonic and Electronic Bandgap Materials, School of Physics and Electronic Engineering, Ministry of Education, Harbin Normal University, Harbin 150025, China

[2] School of Physics and Electronic Information, Yantai University, Yantai 264005, China

Published online: 05 September 2024

heterojunction composite material formed by two materials will show better performance than a single two-dimensional material. Because the performance can be fully compensated through interlayer interaction, showing more excellent characteristics.

In this paper, WSe_2/CuO van der Waals heterojunction materials were prepared by a simple and effective liquid phase exfoliation (LPE) method using WSe_2 and CuO as matrix materials, and then fabricated into SA devices by vacuum filtration and film transfer technology, which were applied to 2 μm Tm: YAP pulsed lasers. In passive Q-switched operation, the best performance was obtained at the central wavelength of 1986.8 nm. When the pump power was 25.46 W, the maximum average output power of the pulse was 2.32 W, the repetition frequency was 68.68 kHz, the minimum pulse width was 752.8 ns, the peak power was 44.92 W, and the single pulse energy was 33.78 μJ. At the same time, in order to prove the potential and performance of heterojunction materials, a comparative experimental study was made on the modulated laser output performance when CuO was used as SA (1.35 μs, 63.14 kHz).

2 Experimental section

2.1 Preparation and characterization of WSe2/CuO heterojunction films

There are many methods for preparing low-dimensional material films. In our experiment, we chose the simple and effective LPE method combined with vacuum filtration transfer technology. The quality of the film finally prepared will be much better than that of the LPE method and more uniform. The preparation process is shown in Fig. 1(a). Take 100 mg of WSe_2 powder and CuO nanosheet powder, respectively, and dissolve them in 100 mL of anhydrous ethanol. At room temperature, water bath ultrasonication is performed for 3 h to promote the breaking of the interlayer van der Waals force. Use a strong magnetic stirrer to stir for 30 min. After the two solutions are mixed, they are subjected to a second room temperature water bath ultrasonication for 1 h. At this time, the ultrasonicated mixed solution is stirred for another 30 min. The purpose of the two stirrings is to fully dissolve the powder in the solvent. The obtained mixed solution is placed in a centrifuge and centrifuged at 4000 rpm for 15 min to remove the bulk material. Use a cellulose acetate membrane with a pore size of 0.22 μm to vacuum filter the upper clear liquid after centrifugation so that the two materials are evenly and fully deposited on the filter membrane, and the cellulose acetate membrane with the deposited material is dried at room temperature for 12 h. Place a blank quartz substrate in a petri dish, place the cellulose acetate film on the quartz substrate, and drip acetone solution that can dissolve the cellulose acetate film along the edge of the petri dish until the page is higher than the quartz substrate. After standing for 30 min, suck out the waste liquid. This step needs to be repeated many times until the cellulose acetate film is completely dissolved. Finally, the SA device is obtained, as shown in Fig. 1(b), and the circled part is the two-dimensional material film.

First, as shown in Fig. 2(a) and (b), the scanning electron microscopy (SEM) images of the WSe_2/CuO heterojunction at the scale of 10 μm and 1 μm fully prove that WSe_2 and CuO have been combined into a heterostructure, in which the sheet material is WSe_2 and the long sheet material is CuO. Figure 3(a) and (b) are transmission electron microscopy (TEM) images of the WSe_2/CuO heterojunction at the scale of 500 nm and 200 nm, respectively. To prove that the image results are the materials prepared in the experiment, by observing the mapping images of the element distribution, it can be seen that the four elements W, Se, Cu, and O are evenly distributed, as shown in Fig. 3(c)-(h). Further, the corresponding Raman vibration peaks of the material were observed by a Raman spectrometer with an excitation wavelength of 532 nm, and the data results are shown in Fig. 4. The wave number position of 248.9 cm^{-1} corresponds to the $E_{2g}{}^1$ vibration peak of WSe_2. Three characteristic Raman vibration peaks of CuO were found at the wave number

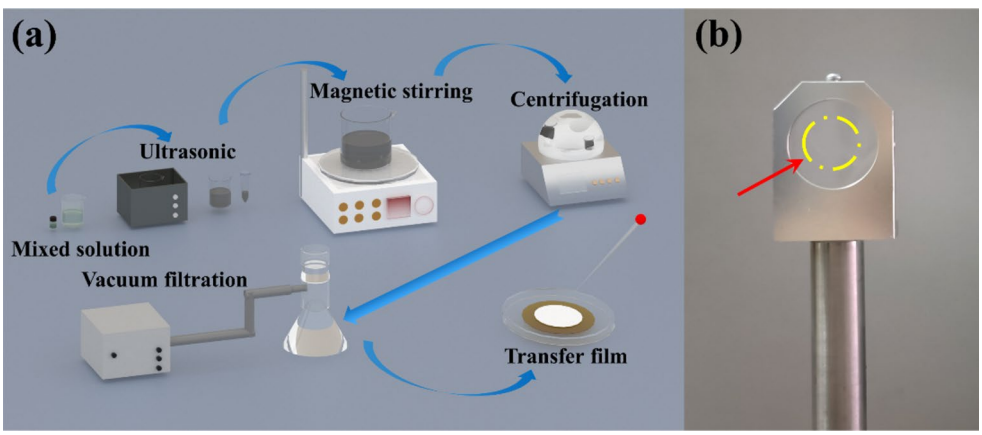

Fig. 1 (**a**) WSe_2/CuO heterojunction preparation flow chart, (**b**) WSe_2/CuO heterojunction SA device

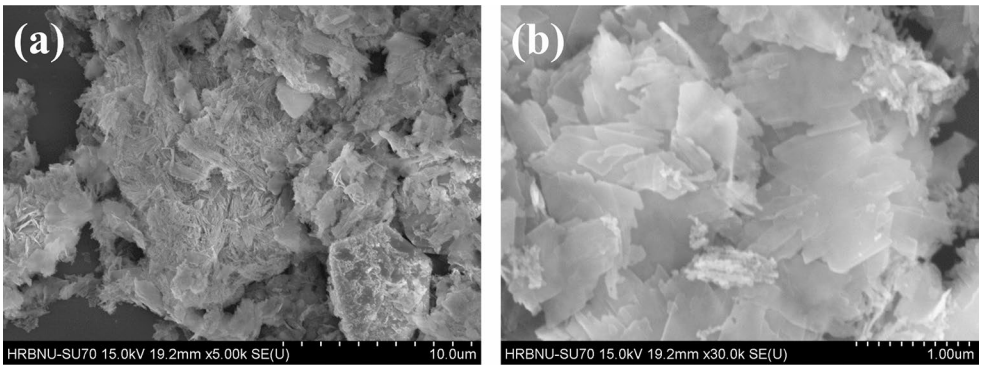

Fig. 2 SEM images of WSe_2/CuO heterostructures at (**a**) 10 μm scale; (**b**) 1 μm scale

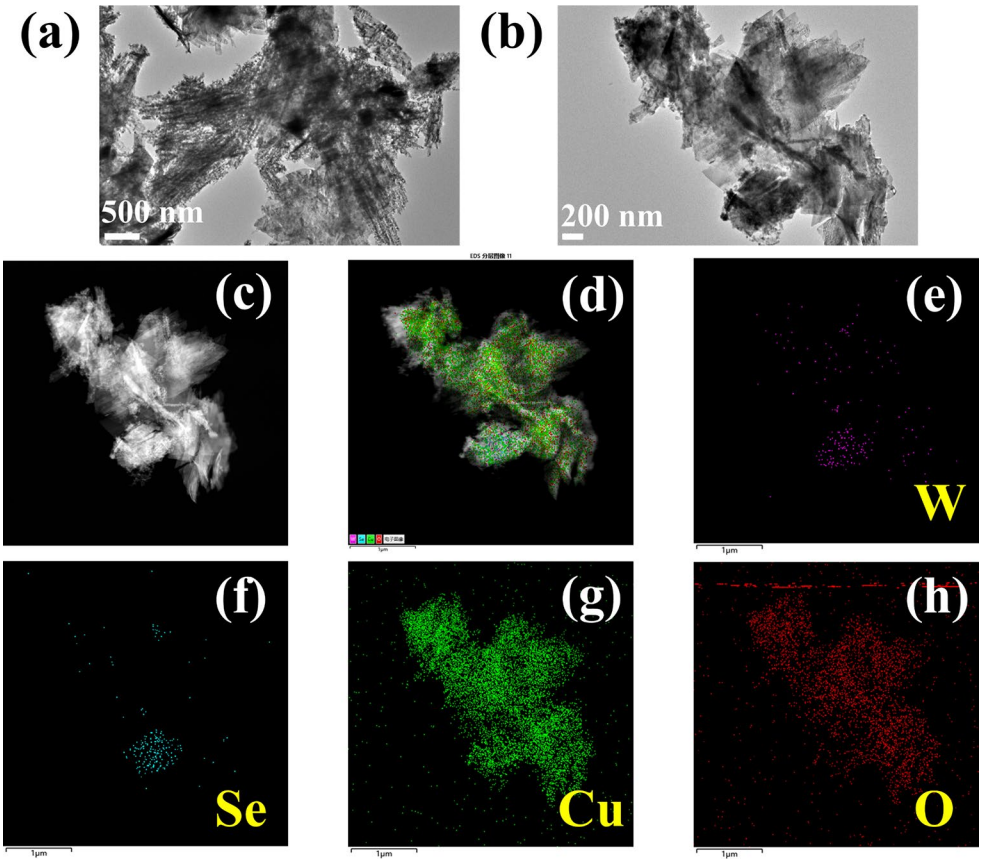

Fig. 3 TEM images of WSe_2/CuO heterostructures at different scales: (**a**) 500 nm, (**b**) 200 nm; EDX layered images: (**c**), (**d**); (**e**)-(**h**) W, Se, Cu, O element mapping images

positions of 278.6 cm^{-1}, 346.4 cm^{-1}, and 631.6 cm^{-1}, which correspond to the vibration modes of A_g, B_g^1, and B_g^2, respectively [31, 32]. It corresponds well with previous research results. Although there is a small shift in the vibration peak position, this is caused by the experimental preparation conditions, but it does not affect the experimental results. XPS technology was used to analyze the WSe_2/CuO heterostructure, and the results are shown in Fig. 5. Figure 5 (a), (b), (c) and (d) show the XPS spectra of W 4f, Se 3d, Cu 2p, and O 1s orbitals, respectively, which are consistent with previous studies [33, 34]. Although there is a small shift in the binding energy peak position, this may be caused by the experimental conditions and environmental conditions and does not affect the experimental results. Based on the above XPS results, it can be found that the sample is mainly composed of WSe_2 and CuO.

2.2 Experimental setup of PQS Tm:YAP laser

In passive Q-switched operation, the laser resonant cavity adopts a straight flat-concave cavity structure, as shown in Fig. 6. A commercial fiber-coupled laser diode (HGLD-792-FH-JC-30 W) with a core diameter of 105 μm and a numerical aperture of 0.22 is used as a pump source, and the operating wavelength is 792 nm. The pump light is focused on the crystal through a collimating and focusing system composed of two lenses. The collimating and focusing system consists of two convex lenses with focal lengths

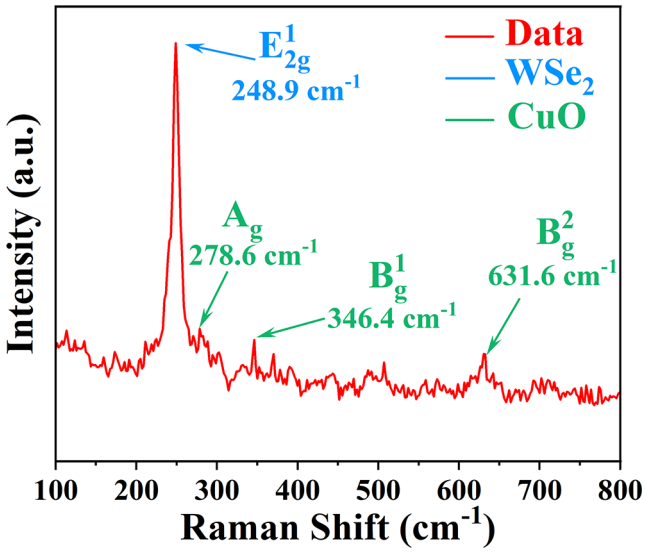

Fig. 4 Raman spectrum of WSe_2/CuO heterojunction

of f1 = 50 mm and f2 = 75 mm and two 45° mirrors that are highly reflective of the pump light. The pump spot radius focused on the crystal is 79 μm. M1 is the input mirror, and the surface is coated with a film layer, which has high transmission at 780–810 nm (T > 99.98%) and high reflection at 1890–2200 nm, (R > 99.98%). The surface of the output coupler (OC) is also coated with a film with high transmittance to pump light, with a transmittance of 5% to laser and a radius of curvature of 200 mm. An a-cut Tm: YAP crystal is selected, with a crystal size of 3 × 3 × 8 mm^3 and a doping concentration of 3 at%. Both end faces of the crystal are coated with a film with high transmittance to pump light and laser. The crystal is wrapped with indium foil and installed in a copper heat conduction device. In order to eliminate heat accumulation, a circulating water chiller is used to cool the pump source and crystal, and the temperature is maintained at 20 °C during the experiment. SA is placed in the cavity near the OC. The length Lc of the PQS resonant cavity is 49 mm.

3 Results and discussion

So far, WSe_2/CuO heterojunction thin film SA has been successfully prepared. In order to prove that the modulation effect of WSe_2/CuO heterojunction is better than that of CuO single material, two sets of experimental results are compared. The power meter used is PM100-19 C. As shown in Fig. 7(a), the output power changes with pump power in continuous wave (CW) mode and PQS mode are recorded. When the LD pump power increases from 3.35 W to 13.80 W, the average output power of the laser operating in CW mode increases from 0.048 W to 3.28 W, and the slope efficiency is 31.6%. In the PQS operation, when CuO is used as SA, the maximum average output power is 1.26 W under the condition of LD pump power of 13.30 W, but when WSe_2/CuO heterojunction is used as SA, the PQS average output power is 2.32 W under the condition of LD pump power of 13.80 W. The slope efficiency is 14.9% and

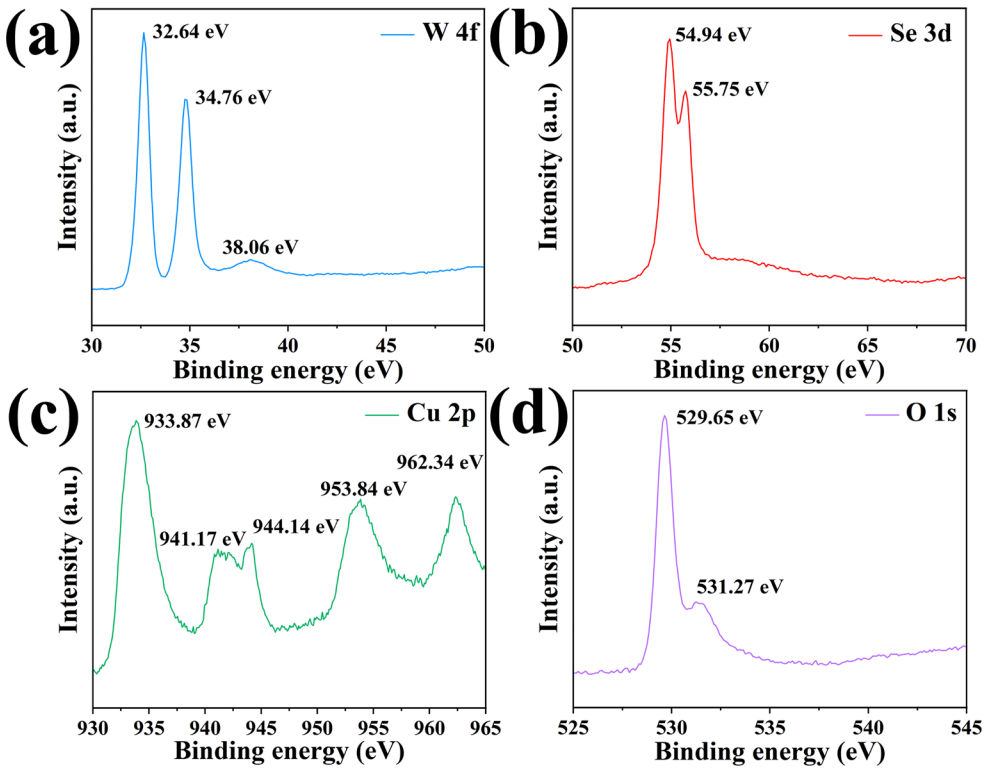

Fig. 5 XPS spectra of WSe_2/CuO heterostructure: (**a**) W; (**b**) Se; (**c**) Cu; (**d**) O

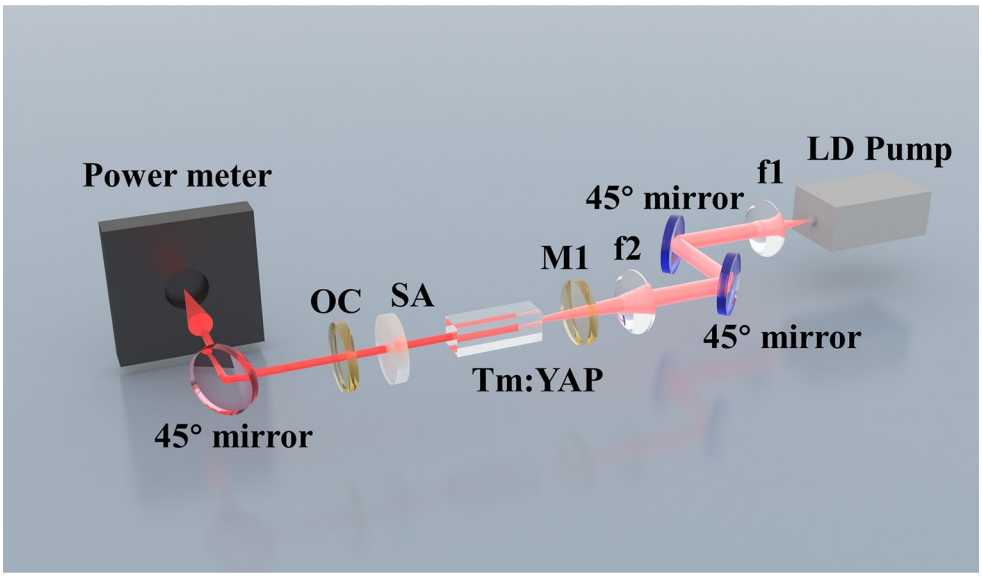

Fig. 6 Diagram of PQS Tm:YAP laser experimental setup

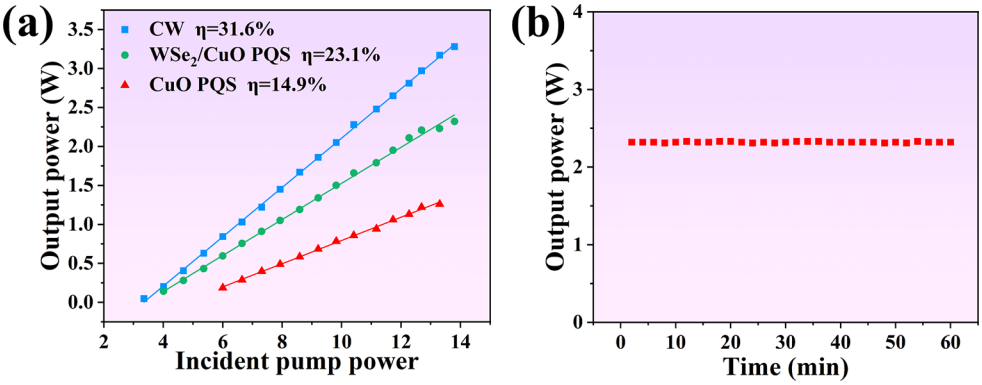

Fig. 7 (**a**) Variation of output power of Tm: YAP laser with pump power in different modes, (**b**) power stability of WSe_2/CuO heterojunction SA PQS laser

23.1% respectively. It can be found that when CuO-SA is used, the threshold pump power is higher and the average output power is lower. This directly indicates that when CuO is inserted, the loss caused is greater, and the use of heterojunction materials is more conducive to the generation of high-power watt-level passive short-pulse lasers. As shown in Fig. 7(b), the output power is recorded every two minutes for one hour, by observing the power stability of the WSe_2/CuO-SA PQS laser, it can be calculated that the coefficient of dispersion is 0.89. It can be shown that the WSe_2/CuO SA PQS laser has very good power stability.

We further studied the pulse response of CuO and WSe_2/CuO heterojunctions. Figures 8 and 9 record in detail the pulse trains and single pulses at the maximum average output power when using the two SAs. The laser pulses were monitored using a digital oscilloscope (KEYSIGHT, DSOX4104, 1 GHz, 5G sample/s) and a high-speed photodetector (EOT, ET5000). As can be seen from the figure, a stable Q-switched state was obtained. For the CuO modulated pulse output, the pulse width was 1.35 μs at an output power of 1.26 W and the repetition rate was 63.14 kHz. When the WSe_2/CuO heterojunction SA was used to generate PQS operation, the pulse width was 752.8 ns at a maximum output power of 2.32 W and the repetition rate was 68.68 kHz. The laser output using heterojunction materials for PQS operation has a narrower pulse width, which fully proves that heterojunction materials are more suitable modulation device materials for short pulse laser output.

We also studied the relationship between the output pulse characteristics and the pump power. The repetition frequencies of the two SA-based lasers increased with the increase of the pump power, and the pulse width showed the opposite trend. This is a typical SA modulation characteristic. Fig. 10(a) and (b) show the changes in the output pulse parameters of the laser when CuO is used as SA. When the pump power increases from 8.59 W to 13.30 W, the pulse repetition frequency increases from 38.75 kHz to 63.14 kHz, and the pulse width decreases from 3.54 μs to 1.35 μs. Both single pulse energy and peak power maintain an upward trend, with changes ranging from 15.1 μJ to 19.96 μJ and 4.16 W to 14.78 W respectively. As shown in the Fig. 10 (c) and (d) shown, when SA is replaced by WSe_2/CuO heterojunction, the output performance is significantly improved. When the pump power increases from

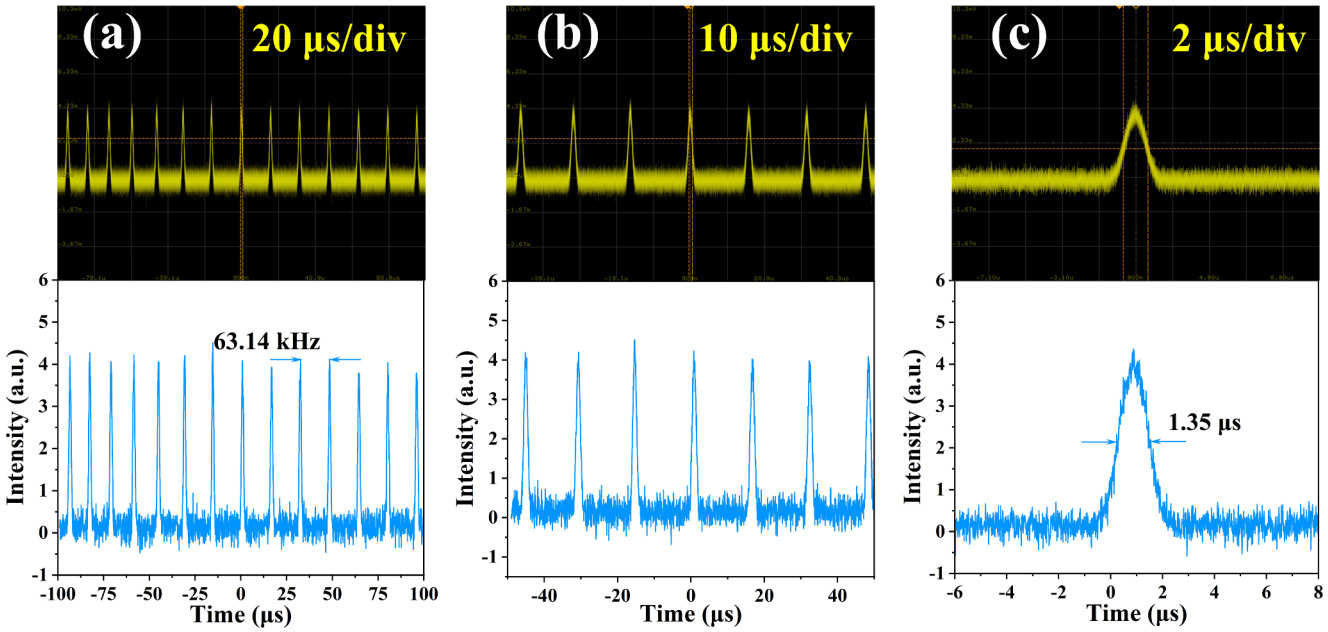

Fig. 8 CuO SA Tm: TAP laser PQS pulse output images at different time scales: (**a**) 20 μs/div; (**b**) 10 μs/div; (**c**) 2 μs/div

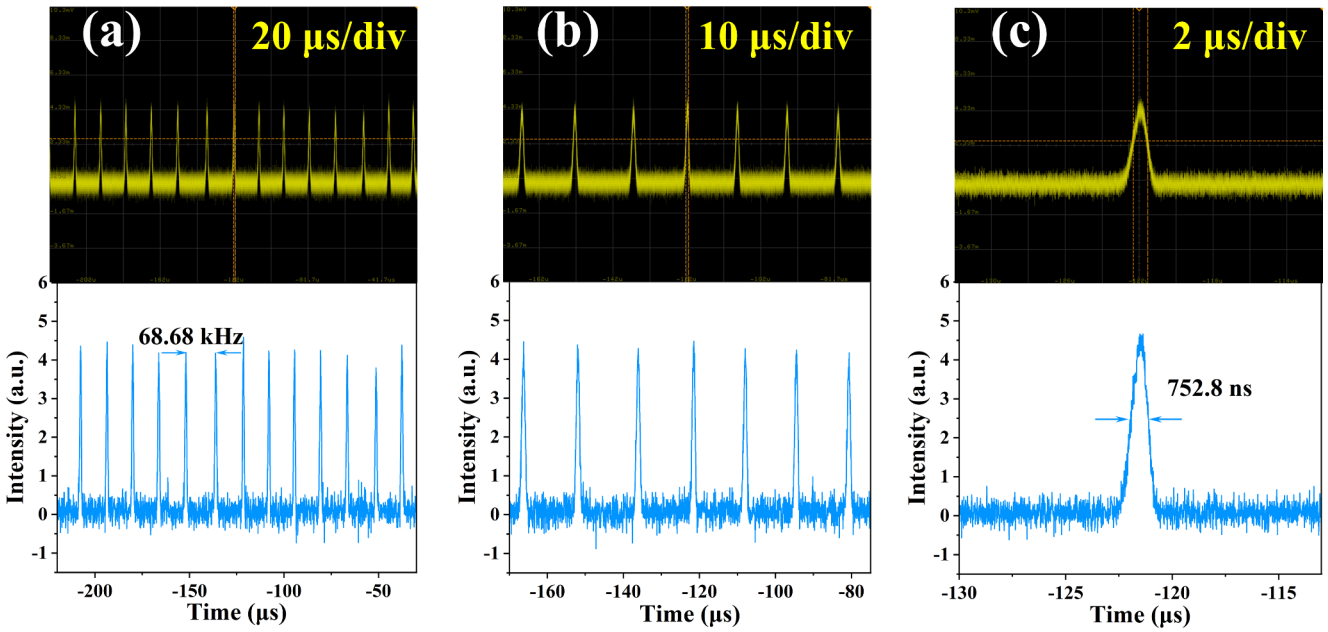

Fig. 9 PQS pulse output images of WSe_2/CuO heterojunction SA Tm: TAP laser at different time scales: (**a**) 20 μs/div; (**b**) 10 μs/div; (**c**) 2 μs/div

8.59 W to 13.80 W, the pulse repetition frequency increases from 51.74 kHz to 68.68 kHz, and the pulse width decreases from 2.45 μs to 752.8 ns. The single pulse energy increased from 23 μJ to 33.78 μJ, and the peak power increased from 9.40 W to 44.92 W. After two sets of experiments, in order to verify that the Q-switching operation was caused by SA, the quartz substrate coated with CuO or WSe_2/CuO heterojunction was replaced with a blank quartz substrate, and no Q-switching pulse signal appeared in the oscilloscope, which indicated that the Q-switching signal was indeed caused by SA. The laser wavelength meter (772B-MIR, Bristol Instruments Inc. USA) was used to measure the output laser center wavelength in different modes. The output spectra of the three lasers under CW mode and CuO and WSe_2/CuO modulation are as shown in the Fig. 11 shown. The central wavelengths are 1995.9 nm, 1987.4 nm, and 1986.8 nm respectively, and the spectral bandwidths of the output spectra in the three modes are 0.11 nm, 0.10 nm, and 0.12 nm respectively. It can be found that compared with the output central wavelength in the CW operation mode, the

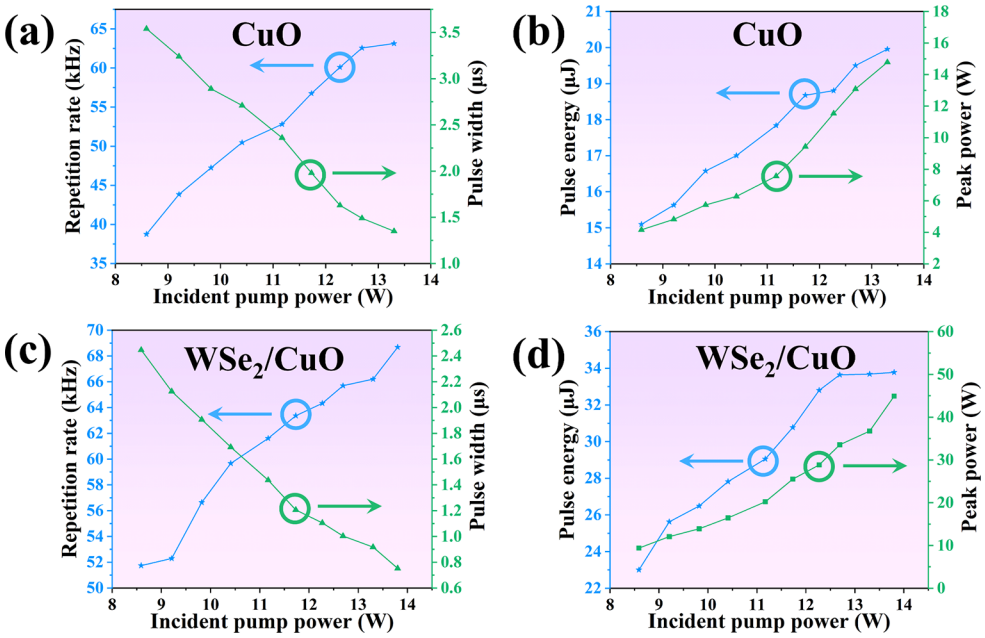

Fig. 10 Pulse output characteristics of two PQS Tm: YAP as a function of pump power: (**a**), (**c**) repetition rate and pulse width; (**b**), (**d**) single pulse energy and peak power

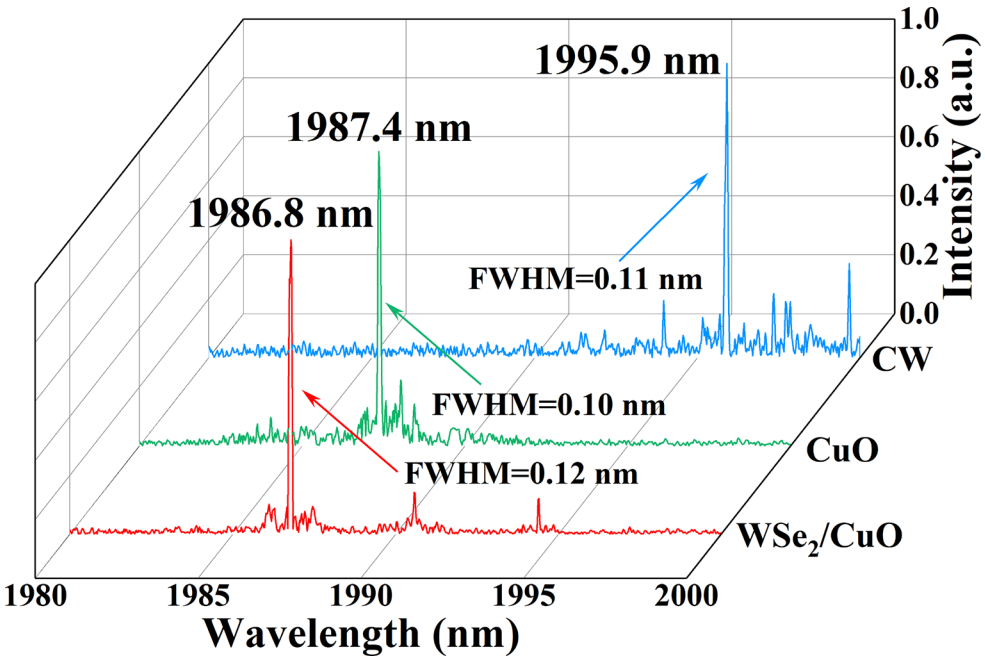

Fig. 11 Output wavelength of Tm: YAP laser in CW and PQS modes

central wavelength in the PQS mode has a blue shift. This is because the energy stored in the emission cross section of the working material in the PQS mode is much greater than that in the CW mode, the emission cross section of the working material becomes narrower, and the central wavelength is blue shifted [35]. At the same time, the nonlinear effect produced when WSe_2/CuO is used as SA also plays a positive role in the blue shift of the center wavelength in the PQS mode [36]. In addition, the number of emission peaks in the output spectrum of the PQS mode Tm: YAP laser is significantly less than that in the CW mode. The main reason is that under the PQS mode operation, the WSe_2/CuO-SA placed in the laser resonator can achieve the effect of Fabry-Perot interferometer, which suppresses the number of laser emission peaks [37–39].

One of the important parameters for evaluating laser output performance is beam quality, which is determined by the value of the beam quality factor M^2. The quality of the pulsed laser beam modulated by SA of the WSe_2/CuO heterojunction was measured using a beam quality analyzer (Thorlabs, BP209-IR2/M), as shown in Fig. 12. Fig. 12(a) shows the M^2 factors in the horizontal and vertical directions obtained by simulating the measured data through the equation, where $Mx^2 = 1.09$ and $My^2 = 1.12$. It can be seen

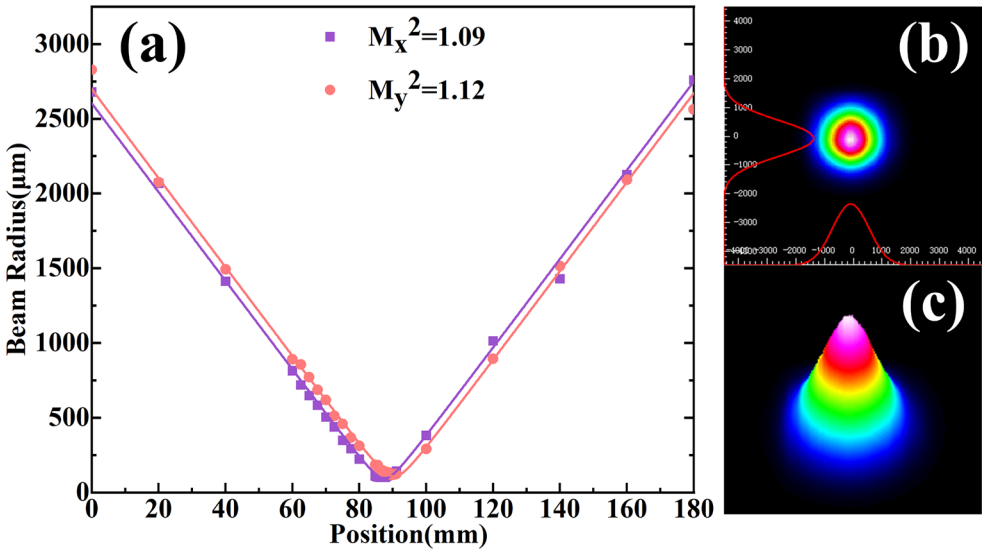

Fig. 12 Output beam quality of PQS laser of WSe_2/CuO heterojunction SA

Table 1 Research results of passively Q-switched all solid-state pulse laser based on WSe_2-SA, and other heterojunction-SAs in 2 μm band

SA	Gain medium	Wavelength (nm)	Pulse width (μs)	Repetition rate(kHz)	Pulse energy (μJ)	Peak power (W)	Output power (W)	Ref.
WSe_2	Tm: YLF	2000	0.427	82	12.8	30	1.51	[40]
WSe_2	Tm: YAP	1988.3	0.393	113.7	11.3	28.9	1.29	[41]
MoS_2/graphene	Tm: YAP	1942	0.473	105	5.267	11.14	0.553	[42]
graphene/BN	Tm: YAP	1934.8	0.607	188.43	19.43	32	3.67	[43]
graphene/WS_2	Tm: YAP	1980.1	1.16	90.36	14.31	12.34	1.293	[44]
Graphene/BN	Ho: YLF	2070	1.56	52	0.73	0.467	0.038	[45]
WSe_2/BN	Tm: YAP	1989.4	1.28	43.51	19.17	14.97	0.834	[23]
WSe2/CuO	Tm: YAP	1986.8	0.753	68.68	33.78	44.92	2.32	This work

that PQS mode has a good beam quality. Fig. 12(b) and (c) show the two-dimensional and three-dimensional light field distribution images of the laser output under Gaussian simulation.

For comparison purposes, the output performance of all-solid-state lasers realized in recent years using a WSe_2 single material, and other heterojunctions of 2D material is shown in Table 1. It can be seen that our results outperform fiber lasers and most solid-state lasers modulated by heterojunctions.

4 Conclusion

In summary, WSe_2/CuO heterojunction composite material SA was prepared by combining LPE method and vacuum filtration method, and then by thin film transfer technology. On this basis, 2 μm PQS laser with WSe_2/CuO heterojunction as SA were constructed for the first time. By comparing the output performance of Tm: TAP pulse laser modulated with single material CuO, it was shown that the composite material has more outstanding and superior modulation performance. In PQS operation, an average output power of 2.32 W and a pulse width of 752.8 ns were achieved. And at a repetition frequency of 68.68 kHz, the maximum single pulse energy is 33.78 μJ and the peak power is 44.92 W. Our work may trigger more thinking about the impact of combining TMDs and TMOs as heterojunctions to prepare optoelectronic devices.

Acknowledgements This work was supported by National Natural Science Foundation of China (NSFC, 61805209).

Author contributions YY wrote the manuscript, LG and YH provided preparation methods, QG provided characterization data, and RL and YS provided editorial guidance and funding for the manuscript.

Data availability No datasets were generated or analysed during the current study.

Declarations

Competing interests The authors declare no competing interests.

Declaration of competing interest The authors declare that they have no known competing financial interests or personal relationships that could have appeared to influence the work reported in this paper.

References

1. W. Du, C. Li, J. Sun, H. Xu, P. Yu, A. Ren, J. Wu, Z. Wang, Laser Photonics Rev. **14**, 2000271 (2020)
2. L. Lv, J. Zhou, Y. Gao, Appl. Phys. Lett. **123**, 160501 (2023)
3. W. Wang, W. Zhai, Y. Chen, Q. He, H. Zhang, Sci. China Chem. **65**, 497 (2022)
4. R. Botella, W. Cao, J. Celis, J. Fernández-Catalá, R. Greco, L. Lu, V. Pankratova, F. Temerov, J. Phys. : Condens. Matter. **36**, 141501 (2024)
5. A. Liu, X. Zhang, Z. Liu, Y. Li, X. Peng, X. Li, Y. Qin, C. Hu, Y. Qiu, H. Jiang, Y. Wang, Y. Li, J. Tang, J. Liu, H. Guo, T. Deng, S. Peng, H. Tian, T.-L. Ren, Nano-Micro Lett. **16**, 119 (2024)
6. N. Vermeulen, S. Palomba, APL Photonics. **4**, 060402 (2019)
7. Y. Xie, M. Chen, Z. Wu, Y. Hu, Y. Wang, J. Wang, H. Guo, Phys. Rev. Appl. **10**, 034005 (2018)
8. Q. Chen, S. Lu, Y. Zhang, H. Yin, Z. Li, P. Zhang, Z. Chen, Opt. Laser Technol. **174**, 110620 (2024)
9. H. Liu, Z. Sun, X. Wang, Y. Wang, G. Cheng, Opt. Express. **25**, 6244 (2017)
10. Z. Qin, G. Xie, J. Ma, P. Yuan, L. Qian, Photon Res. **6**, 1074 (2018)
11. Q. Song, G. Wang, B. Zhang, Q. Zhang, W. Wang, M. Wang, G. Sun, Y. Bo, Q. Peng, Opt. Commun. **347**, 64 (2015)
12. X. Su, B. Zhang, Y. Wang, G. He, G. Li, N. Lin, K. Yang, J. He, S. Liu, Photon Res. **6**, 498 (2018)
13. L. Zhao, C. Zhang, L. Tong, Y. Cai, T. Ning, L. Zheng, J. Lumin. **269**, 120526 (2024)
14. L.O. Amaral, L Daniel-da-Silva Molecules. **27**, 6782 (2022)
15. N. Huo, G. Konstantatos, Nat. Commun. **8**, 572 (2017)
16. D.B. Lioi, D.J. Gosztola, G.P. Wiederrecht, G. Karapetrov, Appl. Phys. Lett. **110**, 081901 (2017)
17. O. Zheliuk, J. Lu, J. Yang, J. Ye, Phys. Status Solidi RRL. **11**, 1700245 (2017)
18. M. Alaloul, J.B. Khurgin, I. Al-Ani, K. As'ham, L. Huang, H.T. Hattori, A.E. Miroshnichenko, Opt. Lett. **47**, 3640 (2022)
19. X. Liu, Z. Hong, Y. Liu, H. Zhang, L. Guo, X. Ge, Opt. Mater. Express. **11**, 385 (2021)
20. A. Singh, Y. Li, B. Fodor, L. Makai, J. Zhou, H. Xu, A. Akey, J. Li, R. Jaramillo, Appl. Phys. Lett. **115**, 161902 (2019)
21. C.Y. Tang, P.K. Cheng, X.Y. Wang, S. Ma, H. Long, Y.H. Tsang, Opt. Mater. **101**, 109694 (2020)
22. R. Wang, J. Han, P. Xu, T. Gao, J. Zhong, X. Wang, X. Zhang, Z. Li, L. Xu, B. Song, Adv. Sci. **7**, 2000216 (2020)
23. L. Gao, X. Zhai, L. Jiang, Q. Sui, D. Niu, Q. Zhang, R. Lan, Y. Shen, Opt. Express. **32**, 3688 (2024)
24. O.K. Arriortua, M. Insausti, L. Lezama, I. Gil, De E. Muro, J.M. Garaio, De La R.M. Fuente, M.P. Fratila, R. Morales, M. Costa, M. Eceiza, Sagartzazu-Aizpurua, J.M. Aizpurua, Colloids Surf., B **165**, 315 (2018)
25. C. Ma, J. Peng, X. Yang, H. Zhang, Q. Zhao, D. Li, X. Su, Y. Zheng, Opt. Commun. **473**, 125979 (2020)
26. A. Naldoni, M. Altomare, G. Zoppellaro, N. Liu, Š. Kment, R. Zbořil, P. Schmuki, ACS Catal. **9**, 345 (2019)
27. L. Pang, R. Wang, L. Li, R. Wu, Y. Lv, Infrared Phys. Technol. **110**, 103444 (2020)
28. Kamakshi. S, Anantha Lakshmi. P, Shenbhagaraman. R, Jenavio Maria Amirtham. P, Siva. R, Lakshmanan. G, Selvakumari. J, Nano Ex. **5**, 025029 (2024)
29. H. Sopha, M. Krbal, S. Ng, J. Prikryl, R. Zazpe, F.K. Yam, J.M. Macak, Appl. Mater. Today. **9**, 104 (2017)
30. L. Dong, H. Chu, X. Wang, Y. Li, S. Zhao, D. Li, Nanophotonics. **10**, 1541 (2021)
31. C. Feng, J. Xiang, P. Liu, B. Xiang, Mater. Res. Express. **4**, 095703 (2017)
32. H. Hagemann, H. Bill, W. Sadowski, E. Walker, M. François, Solid State Commun. **73**, 447 (1990)
33. Y. Wang, S. Zhao, Yi. Wang, D.A. Laleyan, Y. Wu, B. Ouyang, P. Ou, J. Song, Z. Mi, Nano Energy. **51**, 54 (2018)
34. P. Kumar, G.K. Inwati, M.C. Mathpal, S. Ghosh, W.D. Roos, H.C. Swart, Appl. Surf. Sci. **560**, 150026 (2021)
35. L. Li, X. Yang, L. Zhou, W. Xie, C. Xu, Y. Wang, Y. Shen, Z. Lv, X. Duan, Y. Lu, Opt. Laser Technol. **112**, 39 (2019)
36. L. Li, T. Qi, W. Xie, X. Yang, L. Zhou, S. Li, H. Wu, Y. Shen, Infrared Phys. Technol. **119**, 103942 (2021)
37. H. Ahmad, N.A. Roslan, M.K.A. Zaini, M.Z. Samion, Optik. **262**, 169359 (2022)
38. G. Lim, J. Lee, J. Jung, J.H. Lee, Opt. Laser Technol. **157**, 108671 (2023)
39. M. Wang, Y. Huang, L. Yu, Z. Song, D. Liang, S. Ruan, IEEE Photonics J. **10**, 1 (2018)
40. L. Cao, W. Tang, S. Zhao, Y. Li, X. Zhang, N. Qi, D. Li, Opt. Laser Technol. **113**, 72 (2019)
41. L. Li, W. Cui, X. Yang, L. Zhou, Y. Yang, W. Xie, X. Duan, Y. Shen, J. Han, Opt. Laser Technol. **125**, 105960 (2020)
42. X. Wang, J. Xu, Y. Sun, W. Feng, Z. You, D. Sun, C. Tu, Laser Phys. Lett. **15**, 015801 (2018)
43. L. Gao, Y. Ding, X. Zhai, H. Min, G. Liu, R. Lan, Y. Shen, Opt. Laser Technol. **168**, 109852 (2024)
44. X. Zhang, Y. Shi, T. Zong, B. Liu, Y. Mu, L. Liu, J. Russ Laser Res. **44**, 673 (2023)
45. X. Zhai, Y. Ding, H. Min, L. Gao, G. Liu, R. Lan, Y. Shen, Infrared Phys. Technol. **134**, 104851 (2023)